THE JOURNAL OF BIOLOGICAL CHEMISTRY VOL. 289, NO. 17, pp. 11971–11985, April 25, 2014

The Nuclear Pore Complex Function of Sec13 Protein Is Required for Cell Survival during Retinal Development*

Received for publication, January 2, 2014, and in revised form, March 12, 2014 Published, JBC Papers in Press, March 13, 2014, DOI 10.1074/jbc.M114.547190

Xubo Niu[‡], Jian Hong[§], Xiaofeng Zheng[¶], David B. Melville[‖], Ela W. Knapik**, Anming Meng[¶], and Jinrong Peng[‡1]**

*From the [‡]Key Laboratory for Molecular Animal Nutrition, Ministry of Education, College of Animal Sciences, and [§]Institute of Biotechnology, Zhejiang University, Hangzhou 310058, China, the [¶]State Key Laboratory of Biomembrane and Membrane Engineering, Tsinghua-Peking Center for Life Sciences, School of Life Sciences, Tsinghua University, Beijing 100084, China, the [‖]Department of Molecular and Cell Biology, University of California at Berkeley, Berkeley, California 94720-3370, and the **Department of Medicine, Vanderbilt University Medical Center, Nashville, Tennessee 37232*

Background: Sec13 is a core component in both the protein trafficking complex and the nuclear pore complex (NPC).
Results: The role of Sec13 in retina development has been investigated.
Conclusion: The NPC function of Sec13 is essential for retina development.
Significance: This is the first genetic evidence to differentiate the contributions of the two functions of Sec13 during organogenesis.

Sec13 is a dual function protein, being a core component of both the COPII coat, which mediates protein trafficking from the endoplasmic reticulum to the Golgi apparatus, and the nuclear pore complex (NPC), which facilitates nucleo-cytoplasmic traffic. Here, we present a genetic model to differentiate the roles of these two functions of Sec13 *in vivo*. We report that *sec13*^{sq198} mutant embryos develop small eyes that exhibit disrupted retinal lamination and that the mutant retina contains an excessive number of apoptotic cells. Surprisingly, we found that loss of COPII function by oligonucleotide-mediated gene knockdown of *sec31a* and *sec31b* or brefeldin A treatment did not disrupt retinal lamination, although it did result in digestive organ defects similar to those seen in *sec13*^{sq198}, suggesting that the digestive organ defects observed in *sec13*^{sq198} are due to loss of COPII function, whereas the retinal lamination defects are due to loss of the NPC function. We showed that the retinal cells of *sec13*^{sq198} failed to form proper nuclear pores, leading to a nuclear accumulation of total mRNA and abnormal activation of the p53-dependent apoptosis pathway, causing the retinal defect in *sec13*^{sq198}. Furthermore, we found that a mutant lacking Nup107, a key NPC-specific component, phenocopied the retinal lamination phenotype as observed in *sec13*^{sq198}. Our results demonstrate a requirement for the nuclear pore function of Sec13 in development of the retina and provide the first genetic evidence to differentiate the contributions of the NPC and the COPII functions of Sec13 during organogenesis.

COPII vesicles are responsible for mediating protein trafficking from the ER[2] to the Golgi apparatus, whereas NPCs facilitate nucleo-cytoplasmic traffic. Despite their distinct functions within the cell, structural studies have revealed that these two protein complexes share a common ancestral coatomer element that leads to the formation of a similar lattice-like structure (1–3). Sec13 is a member of the WD-repeat protein family and functions as a core component of both the COPII complex in the cytoplasm (4, 5) and the NPCs across the nuclear envelope. Moreover, Sec13 shuttles between the nucleus and the cytoplasm (6). This fact suggests that Sec13 occupies a unique position as a link between these two evolutionarily related fundamental processes.

Sec13 interacts with Sec31 to form the outer cage of the COPII vesicle coat required for vesicular protein transport from the ER to the Golgi apparatus. Studies of zebrafish genetic mutant *sec13*^{sq198} (7) and of the morpholino-mediated gene knockdown approach (8, 9) have shown that the COPII function of Sec13 is essential for the organogenesis of digestive organs and craniofacial cartilage. Sec23 and Sec24 are two inner coat components essential for the formation of the COPII vesicle. Previous reports have shown that mutants or morphants with compromised COPII function, due to a loss of function of Sec23 or Sec24, exhibit diverse developmental defects, including a deformed craniofacial skeleton structure, small eyes, and a defective digestive system (10–13).

NPCs are large macromolecular assemblies comprising about 30 different proteins known collectively as the nucleoporins (Nups) (14, 15). In the NPCs, Sec13 stably interacts with Nup145C (yeast) or Nup96 (vertebrates) and, together with other proteins, forms a lattice (16, 17). The main role of the nuclear pore is to provide a passage to facilitate the nuclear and cytoplasmic transport of mRNA and proteins. Different NPC components have been found to have critical roles in diverse developmental processes, including oogenesis (18), gastrula-

* This work was supported by "973 Program" Grant 2012CB944550 and National Natural Science Foundation of China Grant 31330050 (to J. R. P.). This work was also supported in part by National Institutes of Health Grant R01 DE018477 from NIDCR (to E. W. K.).

[1] To whom correspondence should be addressed: College of Animal Sciences, Zhejiang University, Hangzhou, China 310058. Tel./Fax: 86-571-88982233; E-mail: pengjr@zju.edu.cn.

[2] The abbreviations used are: ER, endoplasmic reticulum; NPC, nuclear pore complex; hpf, hours post-fertilization; Nup, nucleoporin; BFA, brefeldin A; WISH, whole-mount *in situ* hybridization; TEM, transmission electron microscopy; qPCR, quantitative real time-PCR; GCL, ganglion cell layer; ONL, outer nuclear layer; INL, inner nuclear layer; PH3, phosphorylated histone 3; RPE, retinal pigment epithelium; MO, morpholino; PDI, protein-disulfide isomerase.

tion (19, 20), neurogenesis (21), and the formation of digestive organs, pharyngeal cartilage, and eyes (22–24). Specifically, the study of a zebrafish *flotte lotte* (*flo*) mutant that carries a mutation in the *elys* gene showed that, in addition to displaying hypoplastic digestive organs, the *flo* mutant also exhibited a malformed retina due to the failure of proliferating precursors to differentiate neurons from their stem cell niche (22–24). By studying the zebrafish *nup107* mutant, Zheng *et al.* (25) showed that Nup107 is essential for the development of most organs, including pharyngeal cartilage, intestines, and eyes.

Considering that COPII and the NPC are critical components of fundamental cellular processes, it is striking that loss of function of different COPII or NPC components leads to diverse and distinct phenotypes in vertebrates. Because Sec13 plays an important role in the function of both of these complexes, it is uniquely placed to increase our understanding of these complexes and their relationship with each other. A possible approach is to identify which elements of the Sec13 mutant phenotype are due to the loss of the COPII function and which elements are due to the loss of the NPC function or even to determine whether these are distinct phenotypes. To address this question, we used a zebrafish *sec13*^{sq198} mutant caused by a point mutation altering the normal splicing of the *sec13* transcripts, which results in the addition of 8 bp from the seventh intron leading to a frameshift (7). The aberrant *sec13*^{sq198} transcript encodes the mutant protein Sec13^{sq198}, which lacks the C-terminal 85 amino acids of normal Sec13 (7).

Zebrafish retinogenesis is a precisely regulated process involving a number of intrinsic and extrinsic factors and finely tuned regulatory networks (26, 27). As in other vertebrates, a mature zebrafish retina includes one class of glial cells, the Müller glia, six classes of neurons comprising ganglion, amacrine, bipolar, and horizontal cells, and cone and rod photoreceptors. These different cell types are organized into three distinguishable layers demarcated by two plexiform layers as follows: the innermost ganglion cell layer (GCL) is formed by ganglion cells; the inner nuclear layer (INL) is formed by amacrine, bipolar, and horizontal cells, and the outer nuclear layer (ONL) is formed by cone and rod photoreceptors (26).

Here, we report that, in addition to hypoplastic digestive organs, the *sec13*^{sq198} mutant also displayed a small eye phenotype, with the overall structure of the mutant eye, especially its retinal INL-ONL lamination, being affected. Recently, Schmidt *et al.* (28) also reported a small eye phenotype exhibited by Sec13 knockdown morphants. However, they did not explore the possible contribution of the NPC function of Sec13 to this phenotype (28). In this report, we show the following: 1) the retina lamination phenotype in *sec13*^{sq198} is not entirely due to the compromised COPII function, and 2) disruption of the NPCs in the *sec13*^{sq198} retina is the primary cause for developmental defects of the retina. Furthermore, this conclusion is supported by the fact that a zebrafish mutant lacking Nup107 phenocopies the *sec13*^{sq198} retina lamination phenotype. Taken together, our data clearly demonstrate an important role for the NPC function of Sec13 in the process of retinal development.

EXPERIMENTAL PROCEDURES

Zebrafish Strains—All animal procedures were performed in full accordance with the requirements of the Regulation for the Use of Experimental Animals in Zhejiang Province (Ethics Code Permit ZJU2011-1-11-009Y). The fish lines used included the wild-type AB line (WT), *sec13*^{sq198} (7, 29), and *nup107*^{tsu068Gt} (25).

Hematoxylin and Eosin (H&E) Staining—WT, *sec13*^{sq198}, *nup107*^{tsu068Gt}, and different morphants (including standard control MO morphant, *sec31a* ATG MO, and *sec31b* splice MO double morphant) were fixed, embedded, and cryosectioned as described previously (7, 30). After being washed briefly with distilled water, the cryosections were stained with filtered 0.1% hematoxylin solution for 2 min at room temperature (RT). Following a brief wash in distilled water, the sections were treated with 1% acid alcohol for 30 s, washed with water for 4 min, and then counterstained in 0.5% eosin for about 30 s at RT. After being washed with water for 3 min, the sections were gradually dehydrated in 95 and 100% ethanol and then in xylene three times for 15 min each. Finally, the sections were mounted with balsam, and images were taken under a Nikon ECLIPSE 80i microscope. The Sec23b MO- and Sec24C MO-injected embryos were fixed at 120 or 144 hpf, respectively, and embedded in plastic resin, sectioned, and stained with toluidine blue as described previously (31).

Whole-mount in Situ Hybridization (WISH)—WISH was performed as described previously (7). Gene-specific primers were designed based on available information, and RT-PCR products were cloned into pCS2+ vectors. RNA probes *rod opsin*, *blue opsin*, *red opsin*, *brn3b*, *vsx1*, *otx2*, and *rx1* were labeled with digoxygenin (Roche Diagnostics) and used at a concentration of 0.5 μg/ml.

BrdU Incorporation Analysis, PH3 Antibody Staining, and Apoptosis Assay—For the BrdU incorporation assay, embryos at 36 and 48 hpf were injected with 1 nl of 10 mM BrdU solution. Four hours after injection, embryos were harvested for the immunostaining of BrdU-positive cells using an anti-BrdU antibody (AbD Serotec, OBT0030) in a 1:200 dilution as described previously (7). PH3 immunostaining used the polyclonal antibody against PH3 (Santa Cruz Biotechnology, SC-8656-R) in a 1:200 dilution. An apoptosis assay was performed using the *in situ* cell death detection kit, tetramethylrhodamine red (Roche Diagnostics, 12 156 792 910).

mRNA Rescue and Morpholino Mimicking of the sec13^{sq198} *Phenotype*—Full-length *sec13* cDNA was cloned into the pCS2+ vector. The *sec13* mRNA was synthesized using the mMessage mMachine SP6 kit (Ambion, AM1340). Two hundred pg of *sec13* mRNA was injected into the one-cell stage embryos, and the embryos were subjected to bright field microscopy and WISH. The sec13 and sec31a morpholinos (Gene Tools, Philomath, OR), designed to target their respective translation start sites, were used as described previously (7). Two sec31b splicing morpholinos were designed to target the intron 3-exon 4 junction (sec31b-MO1, 5′-GATCAGATTACTCT GAGATGAAGGA-3′) and exon4-intron 4 junction (sec31b-MO2, 5′-GACTACAGAAACGAGCTGTACCTGT-3′), respectively. One nanoliter of Sec13-ATG MO (1 μM),

TABLE 1
Primers used in the qPCR

Gene	Sequence
p53 forward	TggAgAggAggTCggCAAAATCAA
p53 reverse	gACTgCgggAACCTgAgCCTAAAT
D113p53 forward	ATATCCTggCgAACATTTggAggg
D113p53 reverse	CCTCCTggTCTTgTAATgTCAC
mdm2 forward	CTCgCAgTgAgggCAgTgAAg
mdm2 reverse	TCTAggCACgTAgCgggAAgg
cyclin-G1 forward	gCCCTTTACAgTCCAgCCCAAATC
cyclin-G1 reverse	CTgTgCCTCAAgCCTCTCgATgTA
p21 forward	gAAgCgCAAACAgACCAACAT
p21 reverse	gCAgCTCAATTACgATAAAgA
apaf1 forward	CCgggCTgggTgACTgTATTTg
apafl reverse	gTgCTgggTggCCgCTgACT
baxa forward	CAgAgTggCCCgTgAgAT
baxa reverse	gggggTgCCAAAATAACTg
bcl2 forward	gATAgCCCgggTCACTCgTTCAgA
bcl2 reverse	CCAgTggCCCgTTCAggTAgTCAg
caspase8 forward	AgCggCCTCTTggATACTgTCTA
caspase8 reverse	gCCCAAAACTgTgCCCTTCT
fadd forward	gCCCggCTggTggTCTgg
fadd reverse	CACTCgggCgTTCTCCTTCTTgAT
gadd45aa forward	TggCgCTTCAgATTCACTTCACT
gadd45aa reverse	AgCggTTCACTTTTCCCAgAg
puma forward	CACTgCCCCACATCCCCTCACAT
puma reverse	gTACggCCACCCTCTCCACAgC
elf1a forward	CTTCTCAggCTgACTgTgC
elf1a reverse	CCgCTAgCATTACCCTCC

Sec31a-ATG MO (0.75 μM), sec31b-MO1 or sec31b-MO2 (1 μM) was injected into the one-cell stage embryos. A human β-globin morpholino (5′-CCTCTTACCTCAGTTACAATTT-3′) was used in parallel as the standard negative control morpholino.

Fluorescence Microscopy—The zebrafish embryos were fixed, embedded, and cryosectioned. Primary antibodies against NPCs (Abcam, ab24609), serotonin (Sigma, S5545), collagen II (Lifespan Biosciences, LS-C41831), and PDI (Sigma, P7496) were used in a 1:100 dilution and Zpr-1 (Zebrafish International Resource Center) and Sec13 in a 1:300 dilution. Secondary antibodies conjugated with Alexa Fluor 488, 549, and 647 were used in a 1:400 dilution. DAPI was used to label the nuclei. Images were taken under a Leica TCS SP5 confocal microscope and an Olympus FLUOVIEW FV1000 microscope.

Transmission Electron Microscopy (TEM)—The zebrafish embryos were fixed in 2% glutaraldehyde and 1% paraformaldehyde in PBS for 2 h followed by post-fixation in 1% osmium tetroxide for 1 h at RT. Fixed embryos were gradually dehydrated in ethanol and embedded individually into resin blocks, and 50-nm cross-sections were obtained with an Ultracut E Microtome (Leica) and collected on copper grids. This was followed by staining with 5% uranyl acetate and 2% lead citrate. Images were acquired using a Philips CM-10 TEM or a Hitachi H-7650 TEM.

Quantitative Real Time-PCR (qPCR)—For qPCR, the embryos were collected for total RNA extraction, and a reverse transcription was performed using a reverse transcriptase kit (Invitrogen, 28025-021) according to the manufacturer's protocol. The amount of transcribed cDNA was normalized based on *elongation factor 1a* (*elf1a*). Prepared cDNA and gene-specific primers (0.5 μl of each) were added to SsoFast EvaGreen Supermix (Bio-Rad, 172-5201AP). The CFX96 real time system (Bio-Rad) was used to obtain the threshold cycle (C_t) value. The relative expression of each gene was determined after being normalized to *elf1a.* The primer sequences are listed in Table 1.

Protein Analysis—Protein extraction and Western blot were performed as described previously (7). A mouse monoclonal antibody against zebrafish p53 and rabbit monoclonal antibody against GAPDH (Epitomics, 2251-1) were used as described previously (32). The Western blot bands were visualized by SuperSignal West Femto Maximum Sensitivity Substrate (Thermo Scientific, 34096) and quantified with Adobe Photoshop CS5. The ratio was obtained by dividing the value for p53 or Sec13 by the value for GAPDH before being compared.

mRNA Export Assay—WT, *sec13*^{sq198}, *sup107*^{tsu068Gt}, different morphants (including standard control MO morphant and sec31a ATG MO and sec31b splice MO double morphant), and ethanol-treated and brefeldin A-treated embryos were fixed, embedded, cryosectioned, and stored at −80 °C. When used, the sections were washed with 1× cold PBS and refixed with 4% paraformaldehyde for 20 min on ice. Following permeabilization in PBST (with 0.5% Triton X-100) for 10 min on ice, the sections were washed in 2× SSC for 5 min, prehybridized for 1 h at 37 °C, hybridized with Cy3-oligo(dT)$_{50}$ (Invitrogen) at a concentration of 1000 pg/μl overnight at 37 °C, and then washed with 2× SSC at 37 °C three times for 5 min each. Finally, the stained sections were mounted with DAPI. The images were taken under an Olympus Fluoview FV1000 microscope.

Brefeldin A (BFA) Treatment—Five mg/ml BFA (Sigma, B7651) in 100% ethanol was diluted in egg water to make a 1.5 μg/ml final concentration. Embryos at 22 hpf were incubated in BFA solution for about 62 h. The embryos were then fixed for RNA *in situ* hybridization, protein immunostaining, or H&E staining at 84 hpf.

RESULTS

Retinal Lamination Is Disrupted in the sec13^{sq198} *Mutant*—Immunostaining showed that Sec13 was highly expressed in the WT retinal cells but was only barely detectable in the *sec13*^{sq198} mutant retinal cells (Fig. 1*A*), suggesting that Sec13 is likely to play a role in retinogenesis. In addition to exhibiting dysplastic digestive organs as reported previously (7), we found that *sec13*^{sq198} mutant embryos also displayed a small eye phenotype from 72 h post-fertilization (hpf) onward, despite the size of the eyes appearing normal at 48 hpf (Fig. 1*C* and data not shown). Both H&E staining and TEM analysis showed that the WT embryos developed a typical three-layered retina at 72 and 96 hpf (Fig. 1, *D*, *F,* and *H*). In contrast, the INL and ONL in mutant embryos could not be defined, and the ONL appeared lost or greatly diminished (Fig. 1, *E*, *G,* and *I*). In addition, the retinal pigment epithelium (RPE) in mutant embryos was significantly expanded (Fig. 1, *E* and *G*). All of the eye phenotypes exhibited by the *sec13*^{sq198} mutants were identical to those displayed by the *sec13* morphant reported recently (28).

The specification and differentiation of the retinal cell are sequential events and are completed by 72 hpf in zebrafish (26, 28, 33). WISH using probes for *otx2* and *rx1*, the two key genes for early eye development (34, 35), revealed no drastic differences between the WT and mutant embryos at 36 hpf (Fig. 2*A*), suggesting that the initiation of eye development is not affected by *sec13*^{sq198}, likely because Sec13 is a maternal deposited protein (Fig. 1*B*). WISH using the ganglion cell marker *brn3b*, which encodes a member of the POU domain family of tran-

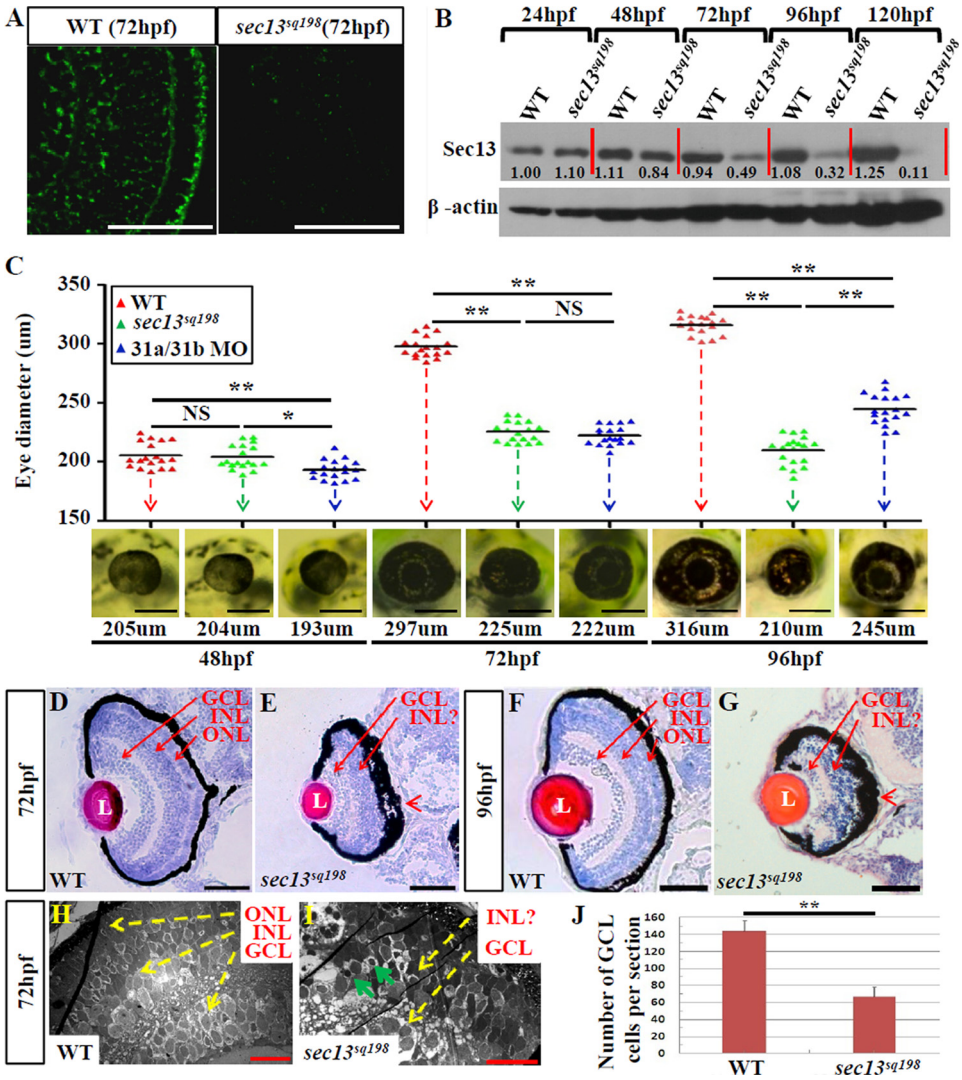

FIGURE 1. **Retinal lamination is disrupted in the *sec13*^{sq198} mutant.** *A*, immunostaining of Sec13 protein in the WT and *sec13*^{sq198} mutant retina at 72 hpf. *B*, Sec13 is a maternal deposited protein. Western blot analysis of Sec13 protein in WT and *sec13*^{sq198} mutant from 24 to 120 hpf is shown. Value for Sec13 protein in WT at 24 hpf is set as 1. *C*, measurements of eye diameter in WT, *sec13*^{sq198} mutant, and *sec31a/sec31b* double morphant at 48, 72, and 96 hpf ($n = 18$). *D–G*, H&E staining analysis of WT (*D* and *F*) and mutant (*E* and *G*) retina at 72 and 96 hpf. WT embryos at 72 and 96 hpf developed normally laminated retinas consisting of a differentiated GCL, an INL, and an ONL (indicated by the *red arrows*). However, retinal lamination in *sec13*^{sq198} mutant embryos was disrupted (indicated by the *red arrows*), and retinal pigment epithelium was clearly expanded in width (shown by the *red arrowheads*). *H* and *I*, TEM analysis of the WT and *sec13*^{sq198} mutant retina at 72 hpf showed that compared with well developed WT retina (*H*), the *sec13*^{sq198} mutant embryos developed disrupted and disorganized retina containing many apoptotic cells (shown by the *green arrows*) (*I*). *J*, average number of GCL cells per section/per embryo in each genotype is shown ($n = 3$, four sections from each embryo were used for counting the GCL cells). *L*, lens. *Scale bar*, 50 μm (*A* and *D–G*), 150 μm (*C*), and 20 μm (*H* and *I*). *NS*, no significance. *, $p < 0.05$; **, $p < 0.01$.

scription factors, showed that a specification of ganglion cells did occur, although the GCL area and number of cells was reduced at 72 hpf (Figs. 1*J* and 2, *B* and *C*). Immunostaining with serotonin (to mark the amacrine cells) and WISH with a *vsx1* RNA probe (to mark the bipolar cells) showed that these two classes of cells were also successfully differentiated (Fig. 2, *D–G*). In the ONL, *rod opsin* expression was barely detectable, and the expression of *red* and *blue opsin* was sharply reduced (Fig. 2, *H–M*) (27, 36). The small eye phenotype and deficiency in the *rod opsin* signal in the ONL were largely rescued by *sec13* mRNA injection and were mimicked in the *sec13* morphant (Fig. 2*N*). Taken together, our results demonstrate that, although retinal cell specification and differentiation are not disrupted in *sec13*^{sq198} mutants, retinal development and the layering of photoreceptors were severely affected. This observation is consistent with that previously observed in the *sec13* morphant (28).

COPII Dysfunction Is Not the Primary Cause of Retinal Lamination Lesions in the sec13^{sq198} *Mutant*—In a previous report, Schmidt *et al.* (28) examined the relationship between opsin secretion and ONL/RPE development, and they concluded that the ONL/RPE lesion resulted from a failure to secrete opsin and collagen in a cell autonomous manner. Sec13 interacts with Sec31 to form the outer coat of the COPII complex, which is critical for protein trafficking from the ER to the Golgi apparatus (37). We found that Sec13^{sq198} mutant protein is a short lived protein *in vivo* (data not shown), and we have previously reported that the Sec13^{sq198} mutant protein lost its ability to form a complex with Sec31 in the cultured human cells, thus disrupting COPII function and leading to cell cycle arrest and

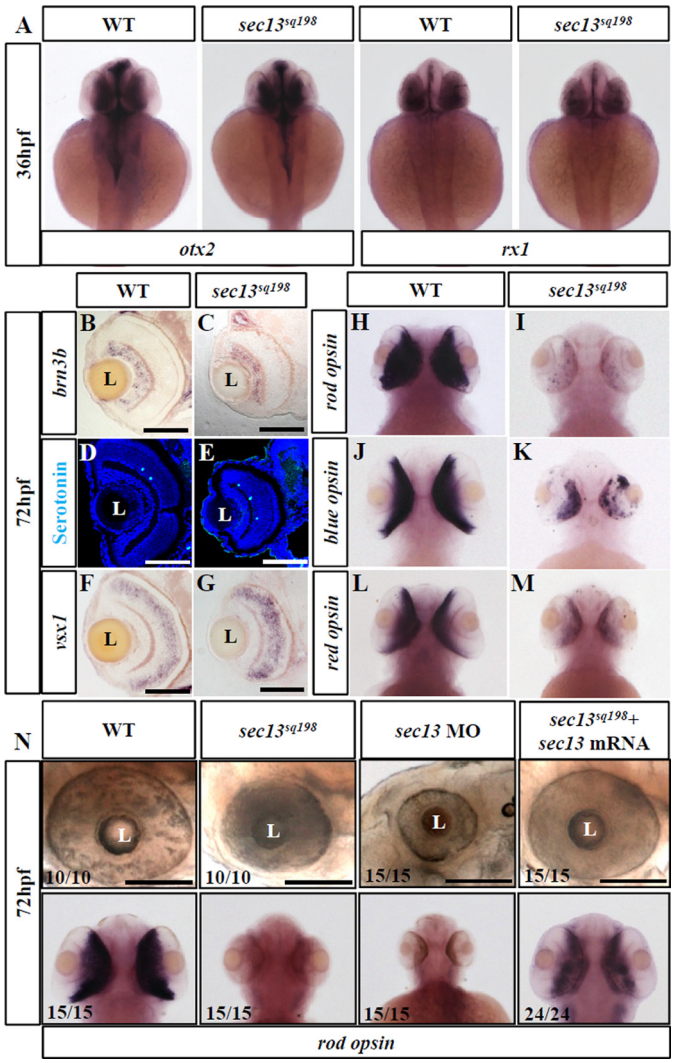

FIGURE 2. **Differentiation of the retinal cells is not affected in the *sec13*^{sq198} mutant.** *A,* WISH analysis of early eye markers *otx2* and *rx1* in the WT and *sec13*^{sq198} mutant embryos at 36 hpf. *B–M, in situ* hybridization analysis of different retinal cell types in the WT and *sec13*^{sq198} mutant at 72 hpf. Examination of each cell type in the WT (*B, D, F, H, J,* and *L*) and *sec13*^{sq198} mutant (*C, E, G, I, K,* and *M*) retina are shown. Ganglion cells were detected with the following: *brn3b* probe (*B* and *C*); amacrine cells with an anti-serotonin antibody (*D* and *E*); bipolar cells with a *vsx1* probe (*F* and *G*); rod photoreceptors with a *rod opsin* probe (*H* and *I*); *blue cones* with a *blue opsin* probe (*J* and *K*); and red cones with a *red opsin* probe (*L* and *M*). *N,* bright field images (*top panel*) of the retina of the WT, *sec13*^{sq198} mutant, *sec13* morphant, and *sec13*^{sq198} mutant embryos injected with *sec13* mRNA at 72 hpf and WISH analysis (*lower panel*) of *rod opsin* expression in the retina of the WT, *sec13*^{sq198} mutant, *sec13* morphant, and *sec13*^{sq198} mutant embryos injected with *sec13* mRNA at 72 hpf. *L,* lens. *Scale bar,* 50 μm (*B–G*) and 150 μm (*N*).

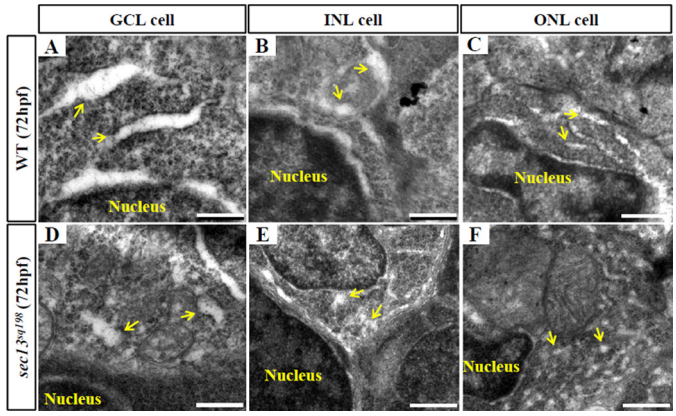

FIGURE 3. **ER lumen in *sec13*^{sq198} mutant retinal cells.** *A–F,* TEM analysis of the ER structure in a GCL cell (*A* and *D*), INL cell (*B* and *E*), and ONL cell (*C* and *F*) in WT (*A–C*) and *sec13*^{sq198} mutants (*D–F*) at 72 hpf. ER lumens are indicated with *yellow arrows*. *Scale bar,* 0.5 μm.

activated apoptosis, which resulted in hypoplasia of the digestive organs in the *sec13*^{sq198} mutant (7). Here, we asked whether the eye defect in the *sec13*^{sq198} mutant is also due to COPII dysfunction. TEM analysis reveals that the ER structure is disrupted in *sec13*^{sq198} mutant retina cells (Fig. 3), albeit to a lesser extent compared with the digestive organs (7). We have also previously shown that knockdown of Sec31a produces even more severe dysplastic digestive organ phenotypes (7). In most vertebrates, including zebrafish, Sec31a has a lone paralog Sec31b. To determine whether the retinal phenotype in the *sec13*^{sq198} mutant was caused by a disruption to the COPII function, we knocked down both Sec31a and Sec31b with their respective specific morpholinos (Fig. 4*A*) (7). We assessed the *sec31a/sec31b* double morphant phenotypes. Like the *sec31a* morphant (7), both the *sec31b* morphant and the *sec31a/sec31b* double morphant displayed small liver, intestine, and pancreas phenotypes (Fig. 4, *B–D*), demonstrating that COPII plays an important role in the organogenesis of the digestive organs. In terms of eye development, the results showed that the *sec31b* morphant exhibited a more profound eye phenotype than the *sec31a* morphant (data not shown). Simultaneous knockdown of Sec31a and Sec31b caused an even more severe eye phenotype (Fig. 1*C*) in addition to a curved body (data not shown). However, the results from H&E staining, WISH using *brn3b* and *vsx1* probes, and immunostaining of Zpr-1 (green/red double cones marker) showed that the co-knockdown of Sec31a and Sec31b did not totally destroy retinal lamination (Fig. 4, *E* and *F*) and cell differentiation (Fig. 4, *G–L*), although it triggered a mild level of cell apoptosis (0.78 apoptotic cells in the standard control MO morphant and 17 in a Sec31a/Sec31b double morphant) (Fig. 4*M*). In fact, previous reports have shown that mutations in *sec24d*, which encodes an inner coat component of the COPII complex, did not cause obvious defects in retinal development in either medaka fish (38) or zebrafish (13), although these mutants were defective in its craniofacial skeleton development. Similarly, the loss-of-function of Sec23a, Sec23b, and Sec24c did not eliminate retinal lamination (Fig. 4, *N–R*) (13, 39).

As an alternative approach to reduce COPII function, we utilized the small molecule BFA (40, 41) and examined its effect on retinal development. BFA is a lactone-type antibiotic drug that inhibits the activation of Arf1 to stop vesiculation at the Golgi, causing Golgi resorption into the ER and effectively preventing all anterograde transport (42, 43). Differentiation of the ganglion cells initiates at about 32 hpf (28), so we treated the embryos at 22 hpf and carried out an analysis at 84 hpf. The efficacy of BFA in blocking COPII function was confirmed by the accumulation of collagen II in the ER, the dilatation of ER lumen in epidermal cells (Fig. 5, *A–F*), and by strong up-regulation of *chop* and *bip* (two ER stress markers) in the brain, eye, and tail, compared with the ethanol-treated control embryos (Fig. 5, *G–J*). BFA treatment caused overall developmental

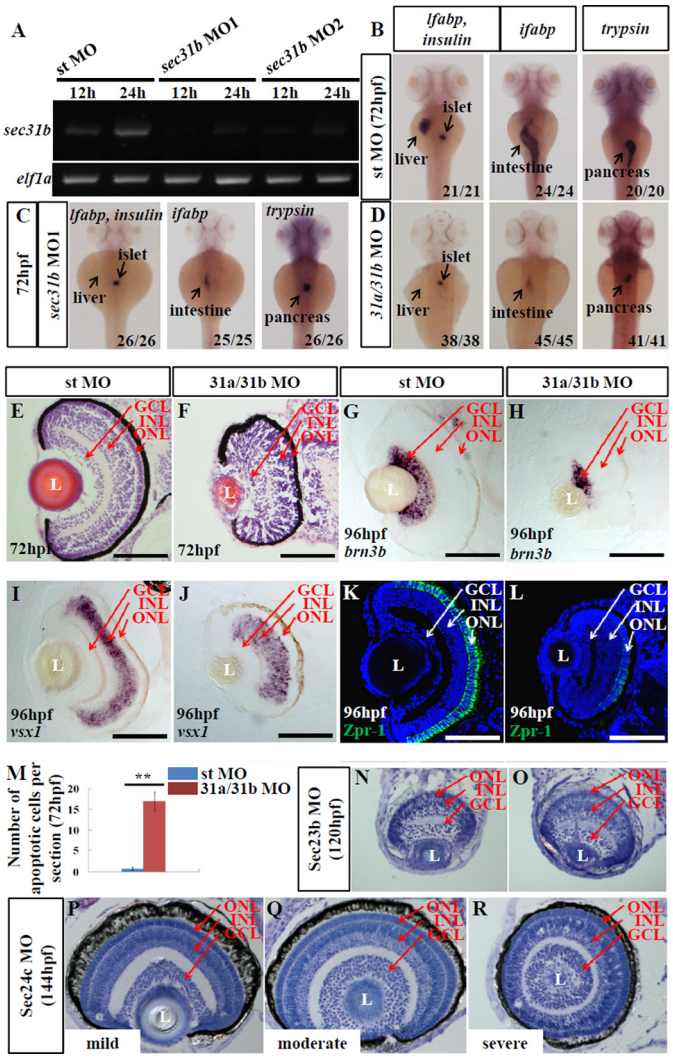

FIGURE 4. **Loss-of-function of COPII does not disrupt retinal lamination.** *A*, expression of *sec31b* in the embryos injected with the standard control morpholino (*st MO*) or two *sec31b* splicing morpholinos (*sec31b* MO1 and *sec31b* MO2) at 12 and 24 hpf were determined by qPCR with the expression of *elf1a* as the normalization control. *B–D*, WISH analysis of digestive organs in the control morphant (*st MO*), *sec31b* morphant, and *sec31a/sec31b* double morphant at 72 hpf. In each case, the number of total embryos examined (as denominator) and the number of embryos exhibiting the displayed phenotype (as numerator) are shown on the *bottom right*. *E* and *F*, H&E staining of the sections of eyes in the control (*E*) and *sec31a/sec31b* double (*F*) morphant. *G–L*, ganglion cells were detected with a *brn3b* probe (*G* and *H*), bipolar cells with a *vsx1* probe (*I* and *J*), and green/red double cones with an anti-Zpr-1 antibody (*K* and *L*). *M*, comparison of the number of apoptotic cells in the control and *sec31a/sec31b* double morphant at 72 hpf ($n = 3$, four sections from each embryo were used for counting the apoptotic cells). *N–R*, histological analysis of the retinal structure in Sec23b morphant at 120 hpf and in Sec24c morphant at 144 hpf. *L*, lens. *Scale bar*, 50 μm (*E–L*).

abnormalities, including shortened body length, heart edema, moderately reduced eye size, and defective digestive organs (Fig. 5, *K–R*), as observed in the *sec31a/sec31b* double morphant. Moreover, BFA treatment triggered apoptosis, mainly in the GCL and INL (on average, 1.5 apoptotic cells in ethanol-treated retina and 53 in BFA-treated retina per section) (Fig. 5, *S–U*). However, unlike the *sec13*^{sq198} mutant, H&E staining, *brn3b* and *vsx1* RNA WISH, and Zpr-1 protein immunostaining all showed that retinal lamination was clearly visible, although Zpr-1 expression was greatly reduced in embryos treated with BFA (Fig. 6, *A–O*). Combined, these data suggest that disruption of the COPII function is not the primary cause of the retinal lamination lesions observed in the *sec13*^{sq198} mutant.

Formation of the Nuclear Pores Is Impaired in the sec13^{sq198} *Mutant Retina*—Sec13 also serves as a key component in NPCs. Because COPII dysfunction did not fully phenocopy the retinal phenotype in the *sec13*^{sq198} mutant, we explored whether the retinal lesion was a result of the combination of the dysfunctions of Sec13's COPII and NPC functions in the *sec13*^{sq198} mutant. To assess the formation of nuclear pores in the retinal cells of the mutant, we performed immunostaining using a mouse Mab414 antibody that recognizes Nup153, Nup214, and Nup358 (44), and we compared the nuclear pores in the WT, *sec31a/sec31b* double morphant, and the *sec13*^{sq198} mutant. At 48 hpf, both the WT and *sec31a/sec31b* double morphant retinal cells showed well formed nuclear pores characterized by a regular ring of these Nups surrounding the nucleus (Fig. 7, *A* and *D*). In contrast, *sec13*^{sq198} mutant retinal cells had an irregular sporadic distribution of Nups (Fig. 7*G*). At 72 and 96 hpf, normal nuclear pores were present in both the WT and *sec31a/sec31b* double morphant retinal cells (Fig. 7, *B*, *C*, *E*, and *F*). In contrast, only a faint signal was detected in the *sec13*^{sq198} mutant at 72 hpf, and the signal was almost undetectable at 96 hpf, suggesting an eventual total disruption of the nuclear pores in the *sec13*^{sq198} mutant (Fig. 7, *H* and *I*). In fact, Western blot of the NPCs using the Mab414 antibody revealed that the levels of proteins in the NPCs were obviously down-regulated in the *sec13*^{sq198} mutant retina (data not shown). Similarly, nuclear pores were also malformed in the mutant digestive organs (Fig. 9, *A–F*), suggesting that dysfunction in the NPCs probably also contributed to the dysplastic digestive organs in *sec13*^{sq198}. We further examined the nuclear pores with TEM. Nuclear pores were clearly visible in all of the retinal cells in the GCL, INL, and ONL in the WT and *sec31a/sec31b* double morphant embryos at 72 hpf (Fig. 7, *J*, *K*, and *M*, and data not shown). However, the number of identifiable nuclear pores in the *sec13*^{sq198} mutant retinal cells in all three layers was markedly reduced (Fig. 7, *L* and *M*, and data not shown).

Total mRNA Accumulates in the Retinal Cell Nucleus in the sec13^{sq198} *Mutant*—Nuclear pores serve as essential channels for the nucleo-cytoplasmic transport of RNA and proteins. Because the formation of nuclear pores was impaired in the *sec13*^{sq198} mutant retinal cells, we wondered whether the export of total polyadenylated mRNA was blocked. We performed fluorescent *in situ* hybridization using Cy3-labeled oligo(dT)$_{50}$ as a molecular probe to determine the cellular distribution of total mRNA. We found that the mRNA was exported out of the nucleus and evenly distributed throughout the cytoplasm in both the WT and *sec31a/sec31b* double morphant retinal cells at 48 hpf (Fig. 8, *A–F*). In contrast, a fraction of the *sec13*^{sq198} mutant retinal cells began to accumulate mRNA in their nuclei at 48 hpf (Fig. 8, *G–I*). By 72 hpf, the nuclear accumulation of mRNA became more prominent in *sec13*^{sq198} mutant retinal cells compared with WT and *sec31a/sec31b* double morphant embryos (Fig. 8, *J–R*). Accumulated mRNAs formed particle-like clusters (Fig. 8, *P–R*). However, BFA treatment neither led to disruption of formation of the NPCs (Fig. 5,

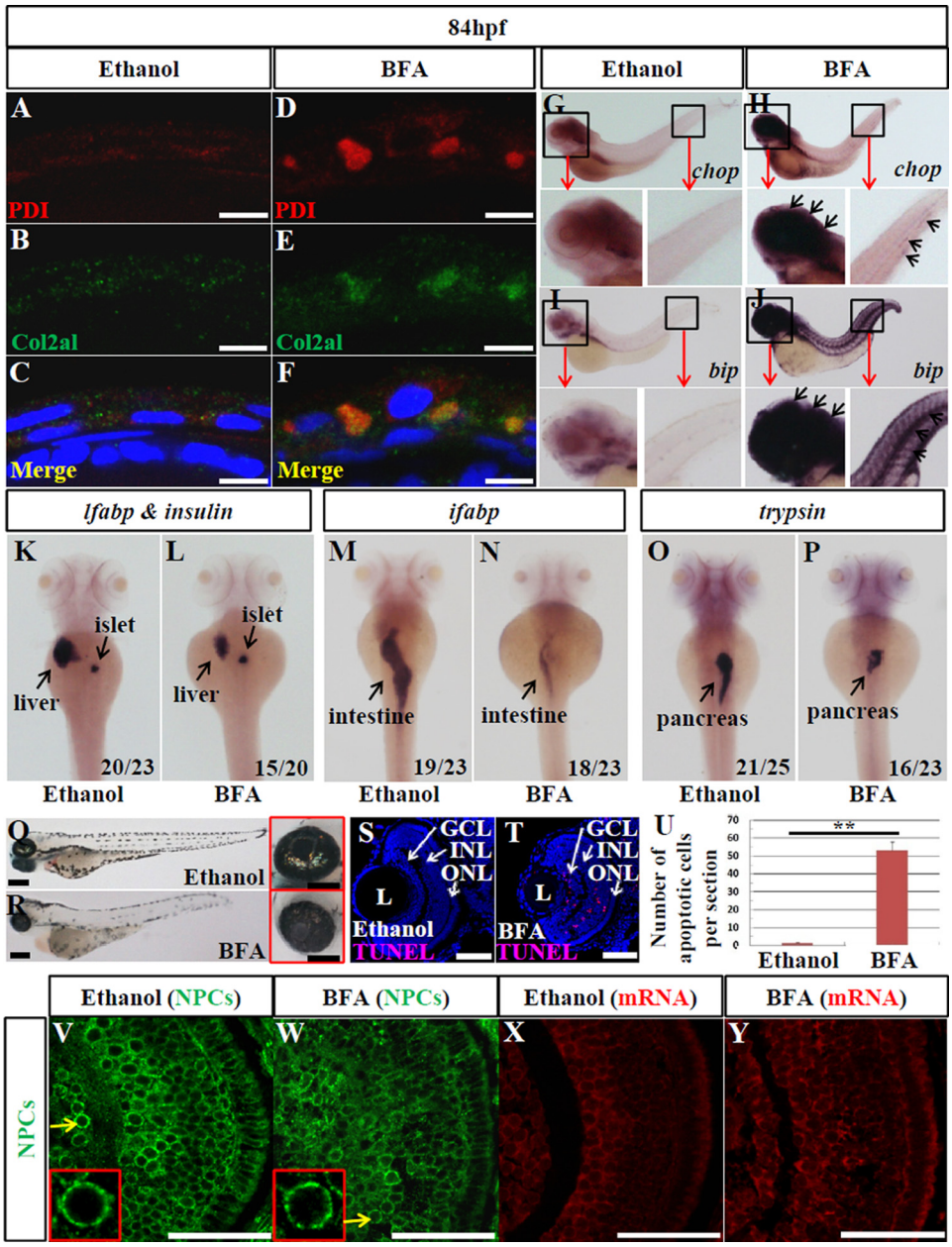

FIGURE 5. **BFA treatment destroys the COPII function and impedes digestive organ development.** *A–F,* double immunostaining of PDI (ER marker) and collagen II (Col2a1, secretory protein) in ethanol-treated (*A–C*) and BFA-treated (*D–F*) embryos at 84 hpf. *A* and *D,* immunostaining of PDI (shown in *red*). *B* and *E,* immunostaining of Col2a1 (in *green*). *C* and *F,* merge of PDI and Col2a1 staining. *G–J,* WISH analysis of *chop* and *bip* in ethanol-treated (*G* and *I*) and BFA-treated (*H* and *J*) embryos at 84 hpf. *K–P,* WISH analysis using *lfabp* (for the liver) plus insulin (for the endocrine pancreas) (*K* and *L*), *ifabp* (for the intestine) (*M* and *N*), and trypsin (for the exocrine pancreas) (*O* and *P*) probes for the analysis of digestive organs in ethanol-treated (*K, M,* and *O*) and BFA-treated (*L, N,* and *P*) embryos at 84 hpf. In each case, the number of total embryos examined (as denominator) and the number of embryos exhibiting the displayed phenotype (as numerator) are shown on the *bottom right*. *Q* and *R,* bright field images of ethanol-treated (*Q*) and BFA-treated (*R*) embryos at 84 hpf. Higher magnification of the eye image is shown on the right correspondingly. *S–U,* representative image of TUNEL analysis of apoptosis in ethanol-treated (*S*) and BFA-treated (*T*) retina at 84 hpf. *U,* average number of apoptotic cells in these samples were shown ($n = 3$, four sections from each embryo were used for counting the apoptotic cells). *V* and *W,* immunostaining of nuclear pores in ethanol-treated (*V*) and BFA-treated (*W*) embryos at 84 hpf. *X* and *Y,* mRNA export assay in ethanol-treated (*X*) and BFA-treated (*Y*) retinas at 84 hpf. *L,* lens. *Scale bar,* 10 μm (*A–F*), 300 μm (*Q* and *R*), 150 μm (*inset* in *Q* and *R*), and 50 μm (*S, T,* and *V–Y*). **, $p < 0.01$.

V and *W*) nor to the accumulation of total RNA of the nuclei in the retina (Fig. 5, *X* and *Y*). These data demonstrate that the NPC function was disrupted in the retinal cells in the *sec13*^{sq198} mutant. Interestingly, we noticed that although the *sec13*^{sq198} mutant's digestive organs exhibited defective nuclear pores, a much smaller number of cells in these organs accumulated total mRNA in the nuclei (Fig. 9, *G–R*).

Loss-of-Function of the NPC Component Nup107 Phenocopies the sec13^{sq198} *Retinal Phenotype*—To better understand the role of NPCs in retinal development, we characterized the *nup107*^{tsu068Gt} mutant, which carries a transposable element insertion in the first intron of *nup107*, a gene encoding another key NPC component (25). Similarly to the *sec13*^{sq198} mutant, the *nup107*^{tsu068Gt} mutant developed a shortened body length,

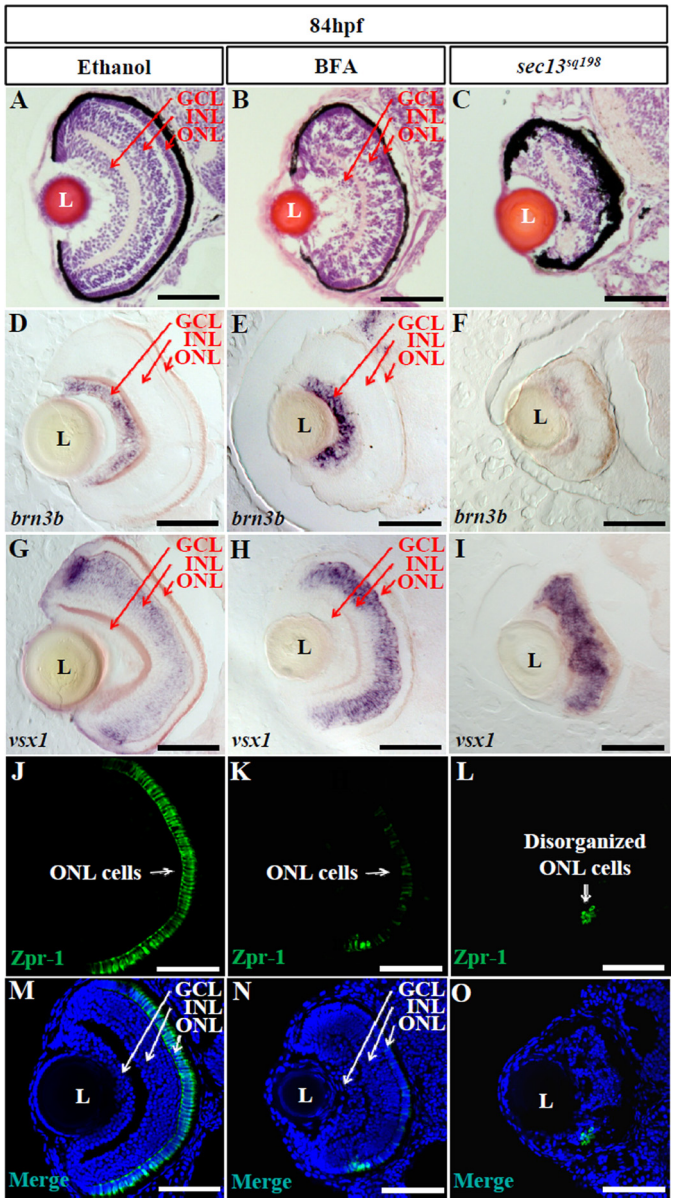

FIGURE 6. **BFA treatment does not disrupt retinal lamination.** *A–C,* H&E staining analysis of the retina in ethanol-treated (*A*), BFA-treated (*B*), and *sec13*^{sq198} mutant (*C*) embryos at 84 hpf. *D–O,* ganglion cells were detected with a *brn3b* probe (*D–F*), bipolar cells with a *vsx1* probe (*G–I*), and green/red double cones with an anti-Zpr-1 antibody (*J–O*). *L,* lens. *Scale bar,* 50 μm.

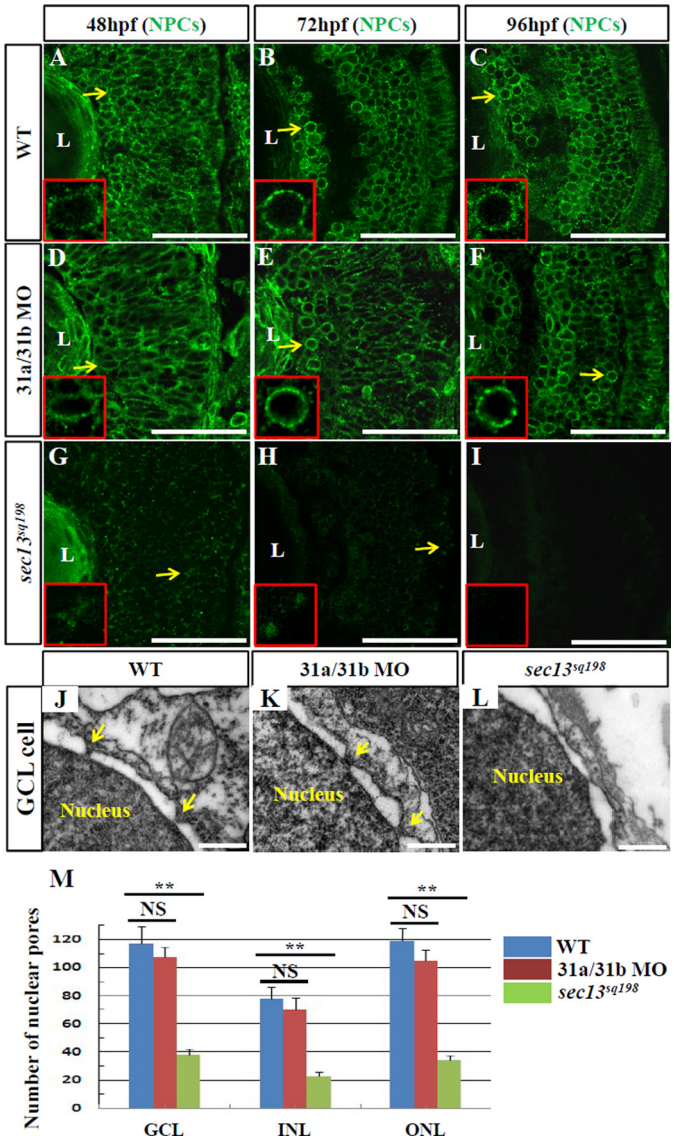

FIGURE 7. **Formation of nuclear pores is impaired in the *sec13*^{sq198} mutant retina.** *A–I,* immunostaining of nuclear pores in WT (*A–C*), *sec131a/sec31b* double morphant (*D–F*), and *sec13*^{sq198} mutant (*G–I*) retina with Mab414 antibody. The nuclear pores in both WT (*A–C*) and the *sec31a/sec31b* double morphant (*D–F*) retina were well formed (shown by the *yellow arrows* and *insets*), whereas formation of the nuclear pores in the *sec13*^{sq198} mutant retina gradually failed (*G–I*) (shown by the *yellow arrows* and *insets*). *J–L,* TEM analysis of the nuclear pores in the GCL cells in WT (*J*), *sec31a/sec31b* double morphant (*K*), and *sec13*^{sq198} mutant (*L*) retina at 72 hpf. Note that both the WT (*J*) and the *sec31a/sec31b* double morphant (*K*) retinal cells displayed characteristic nuclear pores (indicated by the *yellow arrows*). In contrast, the mutant retina was defective in the formation of nuclear pores in cells from all three layers. *M,* comparison of the number of nuclear pores in the GCL, INL, and ONL in the WT, *sec31a/sec31b* double morphants, and *sec13*^{sq198} mutant retina at 72 hpf. Three ultrathin sections from two embryos for each genotype were used to count the number of nuclear pores in the GCL, INL, and ONL, respectively. For each ultrathin section, six cells in each retinal layer were selected for counting, and the total number of nuclear pores from 18 cells in each retinal layer is shown here. *L,* lens. *Scale bar,* 50 μm (*A–I*) and 1 μm (*J–L*). *NS,* no significance. **, $p < 0.01$.

small brain, a defective pharyngeal skeleton, and small eye (Fig. 10, *A* and *B*). H&E staining showed that retinal lamination in the *nup107*^{tsu068Gt} mutant embryos at 84 hpf was severely disrupted, together with a very significant loss of the ONL. This phenotype closely resembled the *sec13*^{sq198} mutant but not the embryos treated with BFA or the *sec31a/sec31b* double morphant (Fig. 10, *C* and *D*). Moreover, similarly to the *sec13*^{sq198} mutant, the formation of nuclear pores was impaired, and polyadenylated mRNA accumulated in the retinal cell nuclei in the *nup107*^{tsu068Gt} mutant (Fig. 10, *E–H*). Immunostaining with Zpr-1 showed that, in contrast to the WT, the *nup107*^{tsu068Gt} homozygous mutant lacked identifiable ONL, and only a few scattered cells expressed Zpr-1 (Fig. 10, *I–N*). This genetic evidence demonstrates that a functional nuclear pore is essential for retinal development.

Activation of the p53-dependent Apoptotic Pathway Contributes to Defective Retinal Lamination in the sec13^{sq198} *Mutant*—Our previous study demonstrated that the hypoplasia of digestive organs in *sec13*^{sq198} mutant embryos was caused by cell cycle arrest and activated apoptosis (7). To explore the cause of the small eye phenotype, we examined cell cycle progression

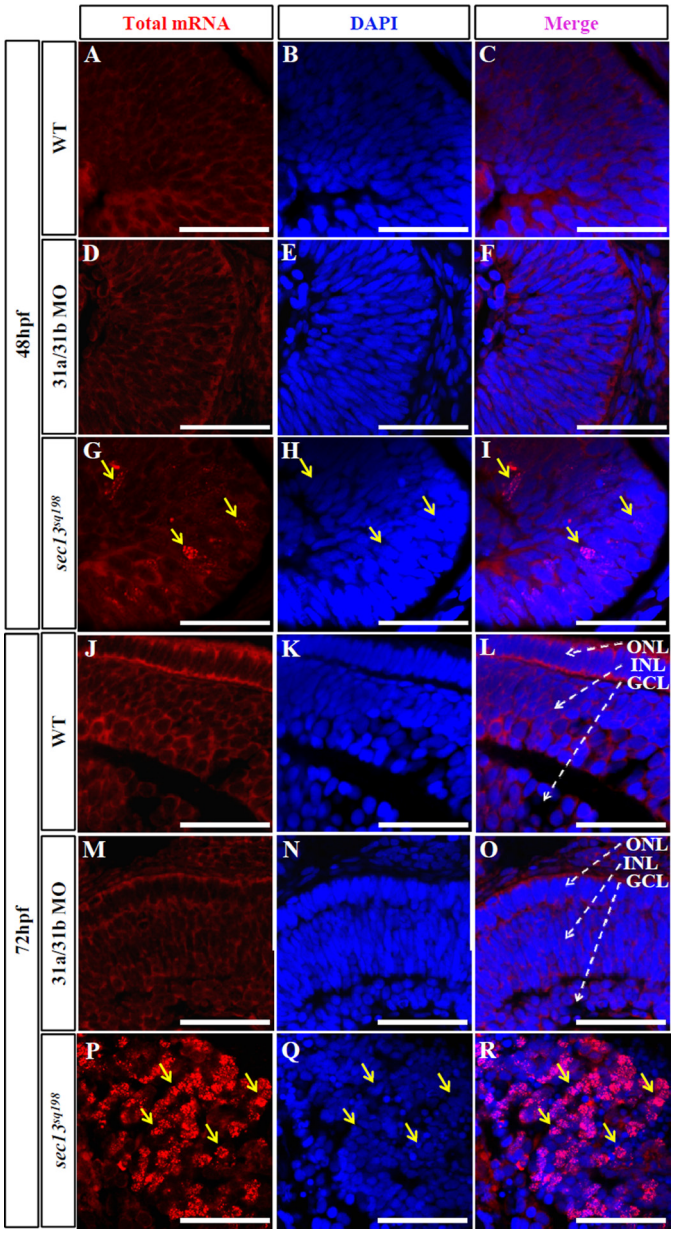

FIGURE 8. **Total polyadenylated mRNAs accumulate in retinal cell nuclei in the *sec13*^{sq198} mutant.** *A–R,* mRNA export assay as marked by Cy3-labeled oligo(dT)$_{50}$ in WT (*A–C* and *J–L*), *sec31a/sec31b* double morphant (*D–F* and *M–O*), and *sec13*^{sq198} mutant (*G–I* and *P–R*) retinas at 48 and 72 hpf. In both WT (*A–C* and *J–L*) and *sec31a/sec31b* double morphant (*D–F* and *M–O*) retinal cells, mRNA was evenly distributed throughout the cytoplasm. However, in the *sec13*^{sq198} mutant retinal cells (*G–I* and *P–R*), export was blocked, and mRNA accumulated in the nuclei (shown by the *yellow arrows*). *Scale bar,* 50 μm.

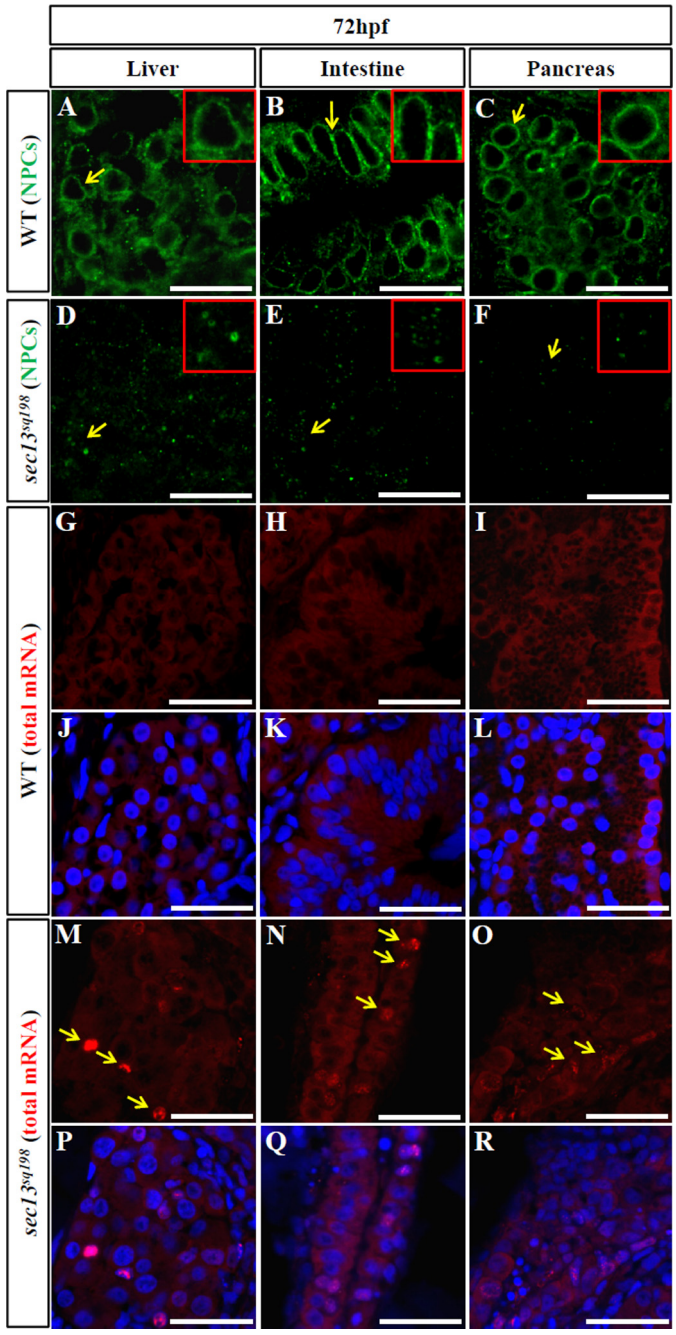

FIGURE 9. ***sec13*^{sq198} mutant digestive organs are also defective in the formation of nuclear pores and mRNA export.** *A–F,* immunostaining of nuclear pores with a mouse monoclonal Mab414 antibody in the WT (*A–C*) and *sec13*^{sq198} mutant (*D–F*) liver, intestine, and pancreatic cells at 72 hpf. *G–R,* mRNA export assay in WT (*G–L*) and *sec13*^{sq198} mutant (*M–R*) liver, intestine, and pancreatic cells at 72 hpf. The nuclei were stained with DAPI. *Scale bar,* 15 μm (*A–F*) and 25 μm (*G–R*).

through immunostaining with PH3 marking M phase cells, and the BrdU labeling assay for S phase cells. We found that PH3-positive cells were located mainly in the peripheral region of the retina at 36 hpf (Fig. 11*A* and data not shown) and at 48 hpf (Fig. 11, *A–C*) in both WT and *sec13*^{sq198} embryos, as reported previously (28). In particular, we consistently observed a small number of PH3-positive cells in the inner layers of the retina in the *sec13*^{sq198} mutant but not in the WT (Fig. 11*C*). No obvious difference in the distribution of BrdU-positive cells was observed between the WT and the *sec13*^{sq198} retina at 40 hpf (BrdU solution was injected at 36 hpf), with BrdU-positive cells being distributed throughout the entire retina (data not shown). At 52 hpf (BrdU solution was injected at 48 hpf), BrdU-positive cells were found in the ONL and the outer half of the INL in the WT retina. In contrast, BrdU-positive cells continued to be present in the entire retina of the *sec13*^{sq198} mutant (data not shown).

To assess the status of cell apoptosis in both WT and mutant retinas, we performed a TUNEL assay. We found almost no apoptotic cells in either WT or mutant retinas (on average, 0.42

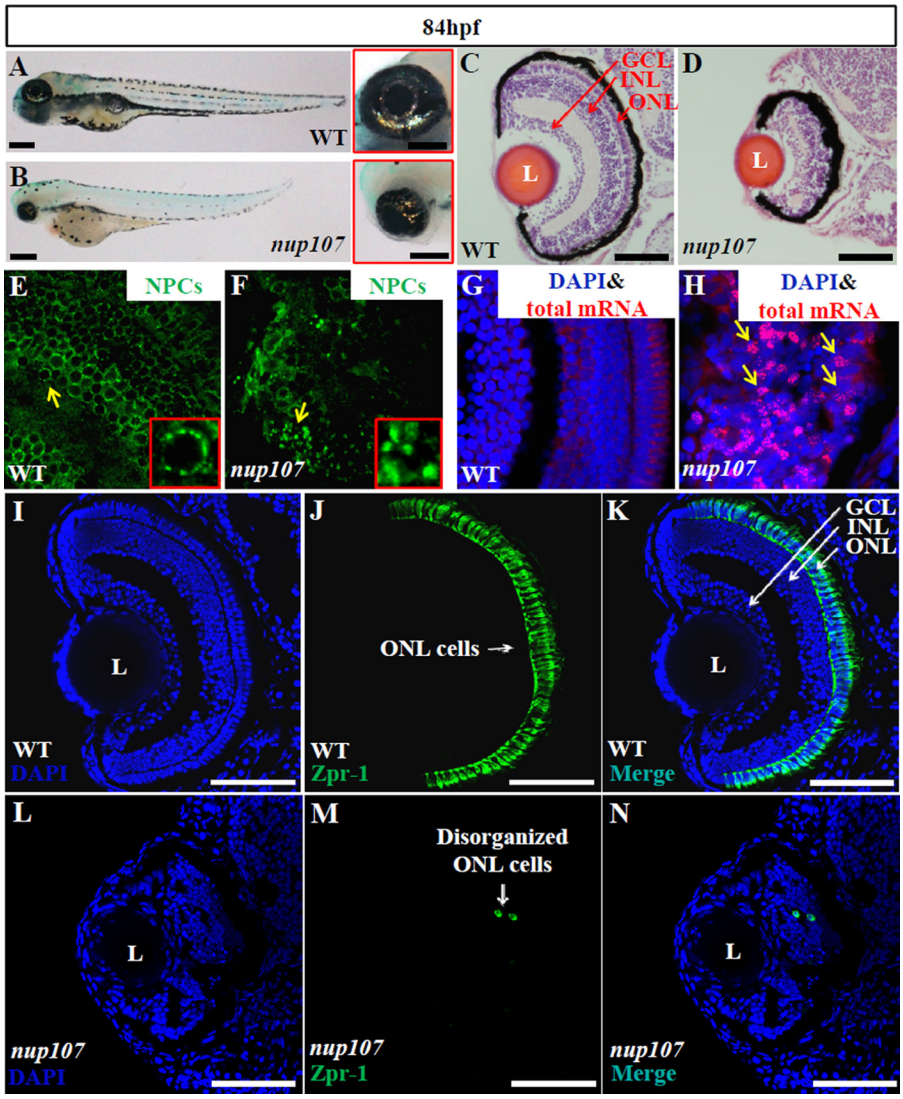

FIGURE 10. **Loss-of-function of the NPC component Nup107 phenocopies the *sec13*^{sq198} retinal phenotype.** *A* and *B*, WT embryo (*A*) and a *nup107*^{tsu068Gt} mutant (*nup107*) embryo (*B*) at 84 hpf. Higher magnification of the eye image is shown on the *right* correspondingly. *C* and *D*, H&E staining analysis of the retina in the WT (*C*) and *nup107*^{tsu068Gt} mutant (*D*) at 84 hpf. *E* and *F*, immunostaining of the NPCs in nuclear pores in WT (*E*) and *nup107*^{tsu068Gt} mutant (*F*) at 84 hpf. *G* and *H*, mRNA export assay in the WT (*G*) and *nup107*^{tsu068Gt} mutant (*H*) at 84 hpf. *I–N*, immunostaining of Zpr-1 in the WT (*I–K*) and *nup107*^{tsu068Gt} mutant (*L–N*) retina at 84 hpf. *L*, lens. *Scale bar*, 300 μm (*A* and *B*), 150 μm (*insets* in *A* and *B*), and 50 μm (*C*, *D*, and *I–N*).

apoptotic cells in WT and 0.33 apoptotic cells in mutant retina per section) at 30 hpf (Fig. 11*D*). However, starting from 48 hpf, some apoptotic cells appeared in the GCL and INL, but rarely in the ONL in the *sec13*^{sq198} mutant (on average, one apoptotic cell in the WT and 31.5 apoptotic cells in the mutant retina per section) (Fig. 11*D*). An excessive number of apoptotic cells was observed in the entire mutant retina by 72 hpf, whereas almost none were found in the WT (on average, 0.58 apoptotic cells in the WT and 139 in the mutant retina per section) (Fig. 11, *D–F*). We also compared the status of cell apoptosis between the WT retina (Fig. 11, *G* and *K*), a BFA-treated retina (with COPII dysfunction) (Fig. 11, *H* and *L*), a *sec13*^{sq198} mutant (with NPC dysfunction) (Fig. 11, *I* and *M*), and a *nup107*^{tsu068Gt} mutant (Fig. 11, *J* and *N*) at 84 hpf. The results showed that both *nup107*^{tsu068Gt} and *sec13*^{sq198} mutants exhibited extensive cell apoptosis coupled with disruption of retinal lamination (Fig. 11, *I, J, M,* and *N*).

A possible outcome of the nuclear accumulation of total mRNA could be the activation of the apoptotic pathway. The tumor suppressor p53 is a well known transcription factor that functions to control the expression of genes involved in promoting cell cycle arrest and cell apoptosis (45). The activation of p53 has been found to be responsible for abnormally elevated apoptotic activity in some zebrafish mutants, including the *flo* mutant (46). Western blot analysis showed that the level of p53 protein was significantly up-regulated in the *sec13*^{sq198} mutant retina (Fig. 12*A*). We then compared the expression of p53-response genes in WT and *sec13*^{sq198} mutant retinas. The result showed that, in addition to *p53*, *Δ113p53*, *p21*, *cyclinG1,* and *mdm2*, genes promoting cell apoptosis, including *caspase8*, *gadd45aa,* and *puma* ,were drastically up-regulated in the *sec13*^{sq198} mutant retina (Fig. 12*B*). These data suggest that significant p53-related cell death occurs in the *sec13*^{sq198} mutant retina. We therefore

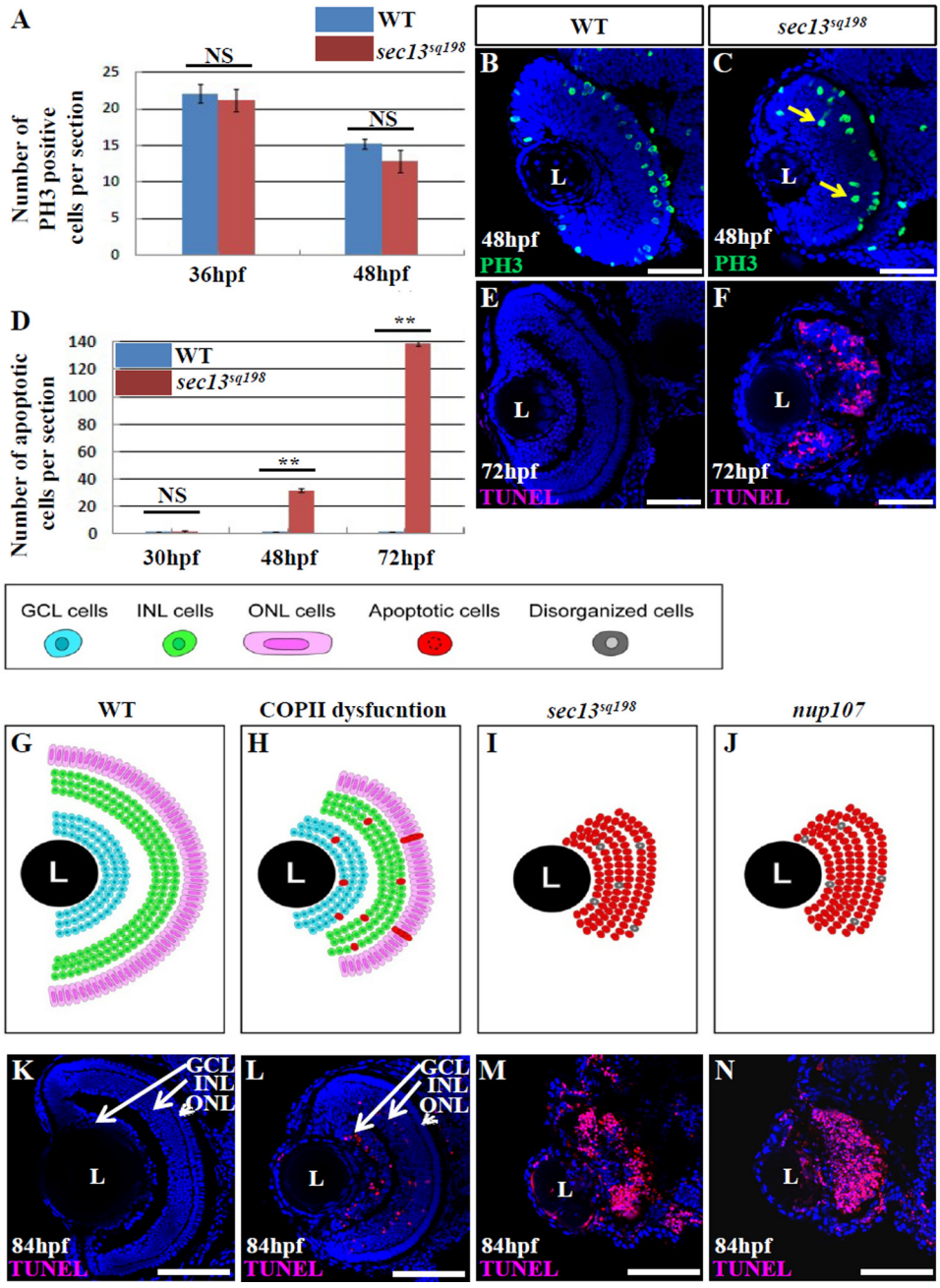

FIGURE 11. **Failure in the formation of nuclear pores triggers cell apoptosis, causing the disruption of retinal lamination in the *sec13*^{sq198} mutant.** *A*, average number of PH3 positive cells per section/embryo in WT and *sec13*^{sq198} mutant retina is shown ($n = 3$, four sections from each embryo were used for counting the PH3-ositive cells). *B* and *C*, representative image of PH3 staining in the WT (*B*) and *sec13*^{sq198} mutant (*C*) retina at 48 hpf. *D*, average number of apoptotic cells in the WT and *sec13*^{sq198} mutant retina at 30, 48, and 72 hpf ($n = 3$, four sections from each embryo were used for counting the apoptotic cells). *E* and *F*, representative image of the TUNEL assays of apoptotic cells in WT (*E*) and *sec13*^{sq198} mutant (*F*) retina at 72 hpf. *G–J*, drawings represent the retinal structure by highlighting the cells in the GCL, INL, and ONL in the WT, BFA-treated (representing COPII-dysfunction), *sec13*^{sq198} mutant, and *nup107*^{tsu068Gt} mutant (representing NPC dysfunction) at 84 hpf. *K–N*, drawings based on TUNEL analysis of apoptotic cells in different genotypes (entire retina). *L*, lens. *Scale bar*, 50 μm. *NS*, no significance. **, $p < 0.01$.

hypothesized that this cell death might be a major contributor to the eye phenotype. To test this, we used the p53 morpholino (47) and performed TUNEL assays on *sec13*^{sq198} mutant embryos injected with p53 morpholino. We found that a knockdown of p53 greatly reduced the number of apoptotic cells (on average, 139 apoptotic cells in the control MO-injected mutant retina and 58 apoptotic cells in the p53 MO-injected mutant retina per section) at 72 hpf (Fig. 12, *C–E*). Strikingly, the knockdown of p53 partially rescued the retinal development, especially the ONL, in the *sec13*^{sq198} mutant eye (Fig. 12, *F–K*).

DISCUSSION

Sec13 serves as a key component in two functional distinct protein complexes, the COPII complex and NPCs, by interacting with distinct partners. Given the importance of these two complexes for normal cellular activities, it would be expected that the COPII and NPC functions of Sec13 are indispensable

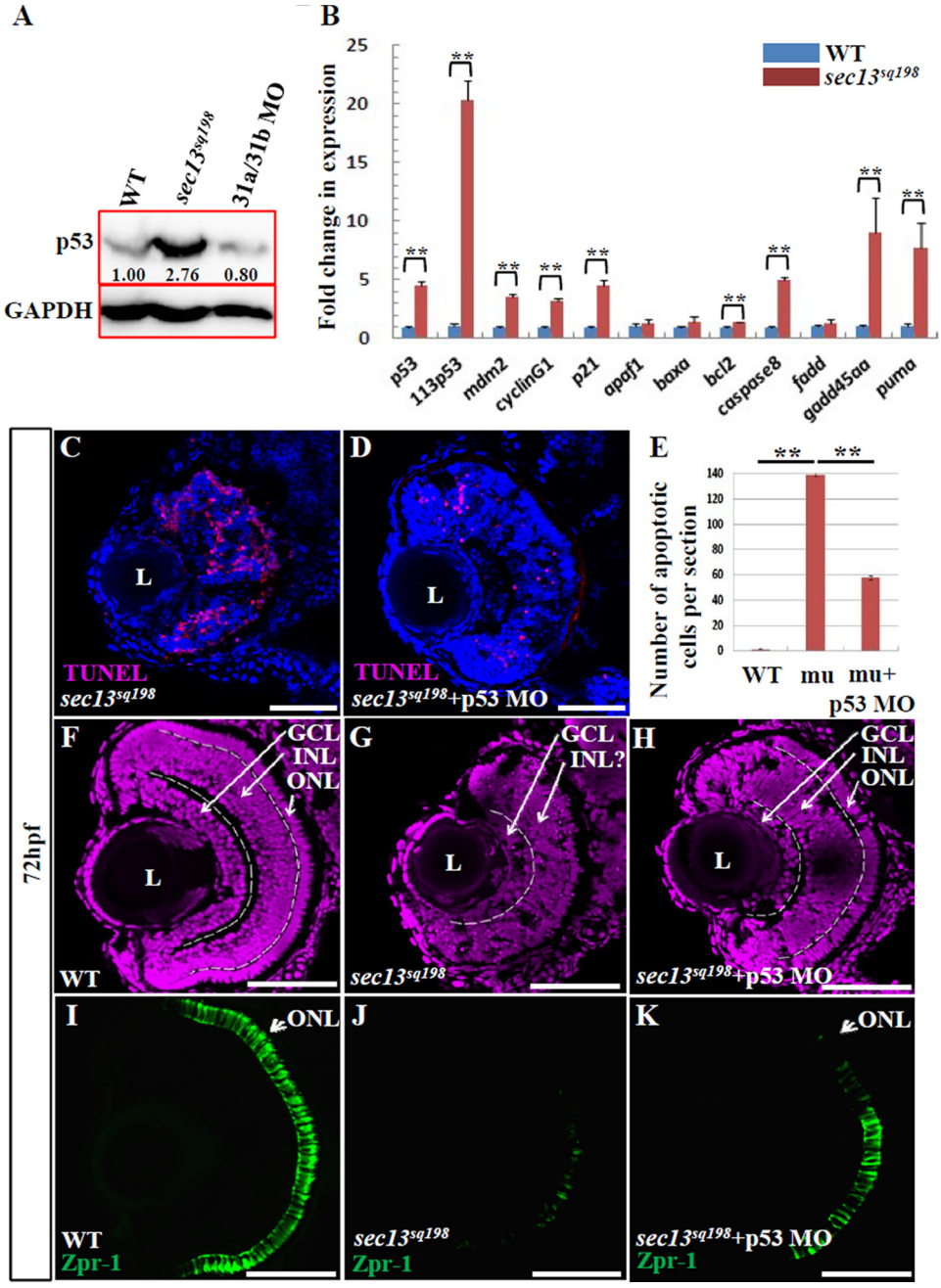

FIGURE 12. **Knockdown of p53 partially restores the *sec13*^{sq198} mutant retina lesion.** *A,* Western blot of p53 protein in the WT, *sec31a/sec31b* double morphant, and *sec13*^{sq198} mutant retina. Value for p53 protein in WT is set as 1. *B,* qPCR analysis of the expression of genes of the p53 and apoptosis pathway in the WT and *sec13*^{sq198} mutant retina. The relative expression level for each gene was expressed as the fold change in expression after normalization against *elf1a*. The *p* value was obtained by performing the two-tailed unpaired *t* test. *C* and *D,* representative image of the TUNEL assays of apoptotic cells in *sec13*^{sq198} mutant (*C*) and p53-ATG morpholino (*p53 MO*)-injected *sec13*^{sq198} mutant (*D*) retina at 72 hpf. *E,* average number of apoptotic cells in the WT, *sec13*^{sq198} mutant, and p53 MO-injected *sec13*^{sq198} mutant retina at 72 hpf ($n = 3$, four sections from each embryo were used for counting the apoptotic cells in each case). *F–H,* overview of the retina in WT (*F*), *sec13*^{sq198} mutant (*G*), and p53 MO-injected *sec13*^{sq198} mutant (*H*) embryos. *I–K,* immunostaining of Zpr-1 in WT (*I*), *sec13*^{sq198} mutant (*J*), and p53 MO-injected *sec13*^{sq198} mutant (*K*) retinas. Clearly, a knockdown of p53 partially restored the layered structure (*H*) (*outlined* with *white lines*) and ONL (*K*) in the *sec13*^{sq198} mutant retina. *L,* lens. *Scale bar,* 50 μm (*C, D,* and *F–K*). **, $p < 0.01$.

for the organogenesis of a specific organ/tissue, although the specific requirement for these two functions is likely to vary in different organs/tissues. However, no genetic model has previously been reported to distinguish these two functions of Sec13 at the level of the whole organism. Comparison of the structure of ER, the formation of NPC, and the distribution of total mRNA revealed that these subcellular organelles are defective both in the retina and digestive organs in the *sec13*^{sq198} mutant at later developmental stages, however, showing different degree of severity in different organs/tissues. Therefore, the *sec13*^{sq198} mutant serves as an ideal genetic model not only for the delineation of the molecular mechanism of the dual Sec13 function in retinogenesis but also in the organogenesis of different organs or, specifically, differentiation of different cell types.

A recent report showed that, in addition to exhibiting defective digestive organ development (9), the knockdown of Sec13

also led to a small eye phenotype (28). Schmidt *et al.* (28) found that the COPII function of Sec13 is essential to the secretion of opsin from the photoreceptor cells and collagen from the RPE to support the development of the ONL and RPE. However, the possible contribution of NPC function of Sec13 to the process of retinal lamination was not explored (28).

We previously reported the identification of the zebrafish *sec13*^{sq198} mutant that exhibited dysplastic digestive organs due to the dysfunction of the COPII complex (7). Here, we showed that the *sec13*^{sq198} mutant also displayed a small eye phenotype with the disruption of retinal lamination at 72 hpf as reported for the *sec13* morphant (28). The relative normal initiation of eye development before 48 hpf in the *sec13*^{sq198} mutant is likely due to the maternal deposited Sec13 protein. However, by 72 hpf, the amount of Sec13 in the *sec13*^{sq198} mutant is not sufficient to support the later developmental events, thus mimicking a conditional genetic model. Surprisingly, our data showed that blocking the COPII function either by a double knockdown of Sec31a and Sec31b or by drug treatment (BFA), despite causing severe defects in the development of the digestive organs and eyes, did not abolish the retinal lamination as observed in the *sec13*^{sq198} mutant. Together with the data obtained in Sec23a, Sec23b, and Sec24c mutants/morphants, we conclude that the COPII dysfunction is not the primary cause of the disruption of retinal lamination in the *sec13*^{sq198} mutant.

Previous reports have demonstrated that NPC activity is essential for development of retinal architecture. For example, mutation of the *elys* gene, which encodes a component of NPCs, not only results in defective digestive organs but also leads to a disrupted retinal structure due to the failure to differentiate the proliferating precursors to neurons from their stem cell niche (22–24). We found that the *sec13*^{sq198} mutant, but not the *sec31a/sec31b* double morphant or the embryo treated with BFA, lacks a nuclear pore structure when examined by TEM and immunostaining of Nup153, Nup214, and Nup358. The structural deficits of the NPCs were accompanied by functional impairment, causing an abnormal accumulation of polyadenylated mRNA in mutant nuclei. The nuclear accumulation of polyadenylated mRNA is likely to ignite a cellular stress response that finally results in an up-regulation of p53-dependent apoptosis in the retinal cells resulting in the defective retinal phenotype. It is notable that the loss-of-function of Elys also activates the p53 pathway to cause apoptosis (24). This is the case for the *nup107*^{tsu068Gt} mutant retina as well (25). Therefore, it appears that comprising NPC function is not compatible with cell viability and the lack of cells in these three different NPC mutants yields lamination defects. This effect is presumably mediated by the p53 pathway because p53 is activated in *elys*$^{-/-}$, *nup107*^{tsu068Gt}, and *sec13*^{sq198} mutants and because down-regulating p53 expression alleviated the *sec13*^{sq198} retinal phenotype. Thus, it can be considered that the p53 pathway is an effector of compromising NPC function. In fact, it is often seen that down-regulation of a downstream effector can fully or partially rescue the mutant phenotype in the mutant background. Reduction in cell apoptosis after p53 knockdown is likely one of the key reasons for the partial rescue of the retinal phenotype in *sec13*^{sq198}. However, it is well known that p53 is a pan-transcription factor that regulates the expression of over 1000 genes. Therefore, in addition to apoptosis, we cannot rule out the possibilities that certain p53 target gene products are involved in regulating retinal lamination.

Interestingly, the loss of the Sec13 function appears to have a more profound effect on the ONL. We hypothesize that the cells in the ONL are probably more sensitive to dysfunction of both the COPII and NPC functions in the Sec13^{sq198} mutant, whereas other types of retinal cells can go through proper differentiation likely due to the presence of the maternal deposited Sec13 protein (7). This scenario is based on the role of Sec13 in the proper formation of nuclear pores to shuttle the mRNAs or proteins necessary for eye development between the nucleus and cytoplasm or in the formation of the COPII complex for protein trafficking. However, we cannot exclude the possibility that Sec13 and other NPC components can act alone or together to mediate specific gene expression to control eye development directly, especially given that the ONL but not the INL and GCL were severely affected in the *sec13*^{sq198} mutant, although total mRNA accumulated in the cells from all three layers. Recently, it has been reported that some NPC members participate directly in the regulation of chromatin organization and gene expression unrelated to their roles in NPCs. For instance, in *Drosophila*, nucleoporins Nup153 and Megator bind to continuous chromosomal regions to modulate gene expression (48). *Drosophila* nucleoporins Sec13, Nup98, and Nup88 were found to occupy ecdysone-induced gene loci (*e.g.* Sgs3 at locus 68C and gene loci 74EF and 75B) during the wandering third instar stage of larval development (49). Similarly, Nup98, Nup50, and Nup62 can directly regulate development and cell cycle genes (*e.g.* VEGF-related factor 2, Sema-2a, CyclinB, and Sak kinase) inside the nucleoplasm in *Drosophila* (50). It was also reported that the deletion of Nup210 blocked myogenesis and neurogenesis, independently of its role in nucleo-cytoplasmic transport (51). Therefore, it is possible that Sec13 teams up with an ONL-specific NPC member to control the expression of genes for the specification of the ONL cells. Future studies will be required to determine whether Sec13 and its partners in the NPCs can directly regulate the expression of genes that are important for the establishment of the eye's architecture.

Acknowledgments—We thank Dr. Jun Chen for valuable suggestions on this project and Dr. Tianhua Zhou for the generous supply of the Zpr-1 antibody.

REFERENCES

1. Brohawn, S. G., Leksa, N. C., Spear, E. D., Rajashankar, K. R., and Schwartz, T. U. (2008) Structural evidence for common ancestry of the nuclear pore complex and vesicle coats. *Science* **322,** 1369–1373
2. Leksa, N. C., and Schwartz, T. U. (2010) Membrane-coating lattice scaffolds in the nuclear pore and vesicle coats: commonalities, differences, challenges. *Nucleus* **1,** 314–318
3. Onischenko, E., and Weis, K. (2011) Nuclear pore complex: a coat specifically tailored for the nuclear envelope. *Curr. Opin. Cell Biol.* **23,** 293–301
4. Antonny, B., and Schekman, R. (2001) ER export: public transportation by the COPII coach. *Curr. Opin. Cell Biol.* **13,** 438–443
5. Stagg, S. M., Gürkan, C., Fowler, D. M., LaPointe, P., Foss, T. R., Potter, C. S., Carragher, B., and Balch, W. E. (2006) Structure of the Sec13/31 COPII coat cage. *Nature* **439,** 234–238

6. Enninga, J., Levay, A., and Fontoura, B. M. (2003) Sec13 shuttles between the nucleus and the cytoplasm and stably interacts with Nup96 at the nuclear pore complex. *Mol. Cell. Biol.* **23,** 7271–7284
7. Niu, X., Gao, C., Jan Lo, L., Luo, Y., Meng, C., Hong, J., Hong, W., and Peng, J. (2012) Sec13 safeguards the integrity of the endoplasmic reticulum and organogenesis of the digestive system in zebrafish. *Dev. Biol.* **367,** 197–207
8. Townley, A. K., Feng, Y., Schmidt, K., Carter, D. A., Porter, R., Verkade, P., and Stephens, D. J. (2008) Efficient coupling of Sec23-Sec24 to Sec13-Sec31 drives COPII-dependent collagen secretion and is essential for normal craniofacial development. *J. Cell Sci.* **121,** 3025–3034
9. Townley, A. K., Schmidt, K., Hodgson, L., and Stephens, D. J. (2012) Epithelial organization and cyst lumen expansion require efficient Sec13-Sec31-driven secretion. *J. Cell Sci.* **125,** 673–684
10. Lang, M. R., Lapierre, L. A., Frotscher, M., Goldenring, J. R., and Knapik, E. W. (2006) Secretory COPII coat component Sec23a is essential for craniofacial chondrocyte maturation. *Nat. Genet.* **38,** 1198–1203
11. Boyadjiev, S. A., Fromme, J. C., Ben, J., Chong, S. S., Nauta, C., Hur, D. J., Zhang, G., Hamamoto, S., Schekman, R., Ravazzola, M., Orci, L., and Eyaid, W. (2006) Cranio-lenticulo-sutural dysplasia is caused by a SEC23A mutation leading to abnormal endoplasmic-reticulum-to-Golgi trafficking. *Nat. Genet.* **38,** 1192–1197
12. Schwarz, K., Iolascon, A., Verissimo, F., Trede, N. S., Horsley, W., Chen, W., Paw, B. H., Hopfner, K. P., Holzmann, K., Russo, R., Esposito, M. R., Spano, D., De Falco, L., Heinrich, K., Joggerst, B., Rojewski, M. T., Perrotta, S., Denecke, J., Pannicke, U., Delaunay, J., Pepperkok, R., and Heimpel, H. (2009) Mutations affecting the secretory COPII coat component SEC23B cause congenital dyserythropoietic anemia type II. *Nat. Genet.* **41,** 936–940
13. Sarmah, S., Barrallo-Gimeno, A., Melville, D. B., Topczewski, J., Solnica-Krezel, L., and Knapik, E. W. (2010) Sec24D-dependent transport of extracellular matrix proteins is required for zebrafish skeletal morphogenesis. *PLoS One* **5,** e10367
14. Beck, M., Förster, F., Ecke, M., Plitzko, J. M., Melchior, F., Gerisch, G., Baumeister, W., and Medalia, O. (2004) Nuclear pore complex structure and dynamics revealed by cryoelectron tomography. *Science* **306,** 1387–1390
15. Alber, F., Dokudovskaya, S., Veenhoff, L. M., Zhang, W., Kipper, J., Devos, D., Suprapto, A., Karni-Schmidt, O., Williams, R., Chait, B. T., Rout, M. P., and Sali, A. (2007) Determining the architectures of macromolecular assemblies. *Nature* **450,** 683–694
16. Lutzmann, M., Kunze, R., Buerer, A., Aebi, U., and Hurt, E. (2002) Modular self-assembly of a Y-shaped multiprotein complex from seven nucleoporins. *EMBO J.* **21,** 387–397
17. Nagy, V., Hsia, K. C., Debler, E. W., Kampmann, M., Davenport, A. M., Blobel, G., and Hoelz, A. (2009) Structure of a trimeric nucleoporin complex reveals alternate oligomerization states. *Proc. Natl. Acad. Sci. U.S.A.* **106,** 17693–17698
18. Senger, S., Csokmay, J., Akbar, T., Tanveer, A., Jones, T. I., Sengupta, P., and Lilly, M. A. (2011) The nucleoporin Seh1 forms a complex with Mio and serves an essential tissue-specific function in *Drosophila* oogenesis. *Development* **138,** 2133–2142
19. Wu, X., Kasper, L. H., Mantcheva, R. T., Mantchev, G. T., Springett, M. J., and van Deursen, J. M. (2001) Disruption of the FG nucleoporin NUP98 causes selective changes in nuclear pore complex stoichiometry and function. *Proc. Natl. Acad. Sci. U.S.A.* **98,** 3191–3196
20. Okita, K., Kiyonari, H., Nobuhisa, I., Kimura, N., Aizawa, S., and Taga, T. (2004) Targeted disruption of the mouse ELYS gene results in embryonic death at peri-implantation development. *Genes Cells* **9,** 1083–1091
21. Lupu, F., Alves, A., Anderson, K., Doye, V., and Lacy, E. (2008) Nuclear pore composition regulates neural stem/progenitor cell differentiation in the mouse embryo. *Dev. Cell* **14,** 831–842
22. de Jong-Curtain, T. A., Parslow, A. C., Trotter, A. J., Hall, N. E., Verkade, H., Tabone, T., Christie, E. L., Crowhurst, M. O., Layton, J. E., Shepherd, I. T., Nixon, S. J., Parton, R. G., Zon, L. I., Stainier, D. Y., Lieschke, G. J., and Heath, J. K. (2009) Abnormal nuclear pore formation triggers apoptosis in the intestinal epithelium of elys-deficient zebrafish. *Gastroenterology* **136,** 902–911
23. Cerveny, K. L., Cavodeassi, F., Turner, K. J., de Jong-Curtain, T. A., Heath, J. K., and Wilson, S. W. (2010) The zebrafish flotte lotte mutant reveals that the local retinal environment promotes the differentiation of proliferating precursors emerging from their stem cell niche. *Development* **137,** 2107–2115
24. Davuluri, G., Gong, W., Yusuff, S., Lorent, K., Muthumani, M., Dolan, A. C., and Pack, M. (2008) Mutation of the zebrafish nucleoporin elys sensitizes tissue progenitors to replication stress. *PLoS Genet.* **4,** e1000240
25. Zheng, X., Yang, S., Han, Y., Zhao, X., Zhao, L., Tian, T., Tong, J., Xu, P., Xiong, C., and Meng, A. (2012) Loss of zygotic NUP107 protein causes missing of pharyngeal skeleton and other tissue defects with impaired nuclear pore function in zebrafish embryos. *J. Biol. Chem.* **287,** 38254–38264
26. Pujic, Z., and Malicki, J. (2004) Retinal pattern and the genetic basis of its formation in zebrafish. *Semin. Cell Dev. Biol.* **15,** 105–114
27. Raymond, P. A., Barthel, L. K., and Curran, G. A. (1995) Developmental patterning of rod and cone photoreceptors in embryonic zebrafish. *J. Comp. Neurol.* **359,** 537–550
28. Schmidt, K., Cavodeassi, F., Feng, Y., and Stephens, D. J. (2013) Early stages of retinal development depend on Sec13 function. *Biol. Open.* **2,** 256–266
29. Huang, H., Ruan, H., Aw, M. Y., Hussain, A., Guo, L., Gao, C., Qian, F., Leung, T., Song, H., Kimelman, D., Wen, Z., and Peng, J. (2008) Mypt1-mediated spatial positioning of Bmp2-producing cells is essential for liver organogenesis. *Development* **135,** 3209–3218
30. Chen, J., Ng, S. M., Chang, C., Zhang, Z., Bourdon, J. C., Lane, D. P., and Peng, J. (2009) P53 isoform delta113p53 is a p53 target gene that antagonizes p53 apoptotic activity via BclxL activation in zebrafish. *Genes Dev.* **23,** 278–290
31. Granero-Moltó, F., Sarmah, S., O'Rear, L., Spagnoli, A., Abrahamson, D., Saus, J., Hudson, B. G., and Knapik, E. W. (2008) Goodpasture antigen-binding protein and its spliced variant, ceramide transfer protein, have different functions in the modulation of apoptosis during zebrafish development. *J. Biol. Chem.* **283,** 20495–20504
32. Tao, T., Shi, H., Guan, Y., Huang, D., Chen, Y., Lane, D. P., Chen, J., and Peng, J. (2013) Def defines a conserved nucleolar pathway that leads p53 to proteasome-independent degradation. *Cell Res.* **23,** 620–634
33. Meyers, J. R., Hu, L., Moses, A., Kaboli, K., Papandrea, A., and Raymond, P. A. (2012) Ss-catenin/Wnt signaling controls progenitor fate in the developing and regenerating zebrafish retina. *Neural Dev.* **7,** 30
34. Bovolenta, P., Mallamaci, A., Briata, P., Corte, G., and Boncinelli, E. (1997) Implication of OTX2 in pigment epithelium determination and neural retina differentiation. *J. Neurosci.* **17,** 4243–4252
35. Chuang, J. C., Mathers, P. H., and Raymond, P. A. (1999) Expression of three Rx homeobox genes in embryonic and adult zebrafish. *Mech. Dev.* **84,** 195–198
36. Nelson, S. M., Park, L., and Stenkamp, D. L. (2009) Retinal homeobox 1 is required for retinal neurogenesis and photoreceptor differentiation in embryonic zebrafish. *Dev. Biol.* **328,** 24–39
37. Fath, S., Mancias, J. D., Bi, X., and Goldberg, J. (2007) Structure and organization of coat proteins in the COPII cage. *Cell* **129,** 1325–1336
38. Ohisa, S., Inohaya, K., Takano, Y., and Kudo, A. (2010) Sec24d encoding a component of COPII is essential for vertebra formation, revealed by the analysis of the medaka mutant, vbi. *Dev. Biol.* **342,** 85–95
39. Melville, D. B., and Knapik, E. W. (2011) Traffic jams in fish bones: ER-to-Golgi protein transport during zebrafish development. *Cell Adh. Migr.* **5,** 114–118
40. Pyati, U. J., Gjini, E., Carbonneau, S., Lee, J. S., Guo, F., Jette, C. A., Kelsell, D. P., and Look, A. T. (2011) P63 mediates an apoptotic response to pharmacological and disease-related ER stress in the developing epidermis. *Dev. Cell* **21,** 492–505
41. Samali, A., Fitzgerald, U., Deegan, S., and Gupta, S. (2010) Methods for monitoring endoplasmic reticulum stress and the unfolded protein response. *Int. J. Cell Biol.* **2010,** 830307
42. Jackson, C. L., and Casanova, J. E. (2000) Turning on ARF: the Sec7 family of guanine-nucleotide exchange factors. *Trends Cell Biol.* **10,** 60–67
43. Nebenführ, A., Ritzenthaler, C., and Robinson, D. G. (2002) Brefeldin A: deciphering an enigmatic inhibitor of secretion. *Plant Physiol.* **130,** 1102–1108

44. Franz, C., Askjaer, P., Antonin, W., Iglesias, C. L., Haselmann, U., Schelder, M., de Marco, A., Wilm, M., Antony, C., and Mattaj, I. W. (2005) Nup155 regulates nuclear envelope and nuclear pore complex formation in nematodes and vertebrates. *EMBO J.* **24,** 3519–3531
45. Amundson, S. A., Myers, T. G., and Fornace, A. J., Jr. (1998) Roles for p53 in growth arrest and apoptosis: putting on the brakes after genotoxic stress. *Oncogene* **17,** 3287–3299
46. Azuma, M., Toyama, R., Laver, E., and Dawid, I. B. (2006) Perturbation of rRNA synthesis in the bap28 mutation leads to apoptosis mediated by p53 in the zebrafish central nervous system. *J. Biol. Chem.* **281,** 13309–13316
47. Chen, J., Ruan, H., Ng, S. M., Gao, C., Soo, H. M., Wu, W., Zhang, Z., Wen, Z., Lane, D. P., and Peng, J. (2005) Loss of function of def selectively up-regulates Δ113p53 expression to arrest expansion growth of digestive organs in zebrafish. *Genes Dev.* **19,** 2900–2911
48. Vaquerizas, J. M., Suyama, R., Kind, J., Miura, K., Luscombe, N. M., and Akhtar, A. (2010) Nuclear pore proteins nup153 and megator define transcriptionally active regions in the *Drosophila* genome. *PLoS Genet.* **6,** e1000846
49. Capelson, M., Liang, Y., Schulte, R., Mair, W., Wagner, U., and Hetzer, M. W. (2010) Chromatin-bound nuclear pore components regulate gene expression in higher eukaryotes. *Cell* **140,** 372–383
50. Kalverda, B., Pickersgill, H., Shloma, V. V., and Fornerod, M. (2010) Nucleoporins directly stimulate expression of developmental and cell-cycle genes inside the nucleoplasm. *Cell* **140,** 360–371
51. DeAngelis, R. A., Markiewski, M. M., Kourtzelis, I., Rafail, S., Syriga, M., Sandor, A., Maurya, M. R., Gupta, S., Subramaniam, S., and Lambris, J. D. (2012) A complement-IL-4 regulatory circuit controls liver regeneration. *J. Immunol.* **188,** 641–648